Bull. Chem. Soc. Jpn., 70, 847—858 (1997)

Molecular-Dynamics Study of Aqueous Solution of Trehalose and Maltose: Implication for the Biological Function of Trehalose

Minoru Sakurai,* Masashi Murata, Yoshio Inoue, Akihiro Hino,† and Syouichi Kobayashi†

Department of Biomolecular Engineering, Tokyo Institute of Technology, 4259 Nagatsuta-cho, Midori-ku, Yokohama 226

†National Food Research Institute, Ministry of Agriculture, Forestry and Fisheries, Kan-nondai, Tsukuba, Ibaraki 305

(Received October 9, 1996)

Molecular-dynamics simulation of aqueous solution of trehalose and maltose were performed to reveal any difference in the hydration ability between them, and to obtain information about how trehalose protects biological materials from water stress. Here, in order to examine the spatial distribution of water molecules around the hydroxy oxygen of sugar, a two-dimensional pair distribution function was introduced in addition to the conventional radial-distribution function. Both sugars were found to be extensively hydrogen bonded to solvent molecules. However, in a solution of maltose, defective hydrogen bonding was found at the exocyclic hydroxymethyl group of the reducing residue. Thus, maltose has a smaller value in hydration number than does trehalose. The translational diffusion of water molecules around trehalose has been found to be slightly more restrained than that around maltose. These findings are consistent with available experimental data concerning the solution properties of both sugars. On the basis of these results, the functional mechanism of tolerance is briefly discussed.

The disaccharide trehalose (α-D-glucopyranosyl α-D-glucopyranoside) has attracted much attention in a variety of scientific fields, including biology,[1—8] food science,[9] and medical science.[10] The integrity and function of biological materials, such as membranes and proteins, are maintained through a freeze-thawing or a freeze-drying process when they are treated together with trehalose.[11] Other mono- and di-saccharides share similar properties.[12] However, various in vitro studies have indicated a higher potency of trehalose as a protecting agent for desiccation.[12,13]

At least two hypotheses have been proposed to explain the molecular mechanism of desiccation tolerance induced by sugar. Under extremely dehydrated conditions, hydroxy groups of sugar are directly hydrogen bonded to the head groups of a lipid. This is called the water-replacement hypothesis.[11,12] The other hypothesis states that a sugar–water mixture is vitrified during dehydration, leading to capsulation of the membrane or protein.[14,15] Which mechanism is responsible for desiccation tolerance in a given system would depend on the relative strength among sugar–lipid, sugar–water, and water–lipid interactions. In any case, the sugar–water interaction is a key factor for determining the ability of sugar as a stress-tolerance inducer.

Evidence has accumulated that trehalose exerts stronger perturbations on the water structure than do other representative disaccharides (maltose and sucrose). Our ^{17}O NMR study has indicated that the rotational motion of water around trehalose is more restricted than those around maltose or sucrose.[16] According to other experimental studies using differential scanning calorimetry (DSC)[16] and ultrasound[17] measurements, an aqueous solution of trehalose possesses a greater amount of unfrozen water per residue, a larger magnitude of partial molar compressibility and a greater amount of hydration water than those of maltose and sucrose. In addition, the concentrated aqueous solution of trehalose exhibits a higher vitrification temperature than those of the others.[18] To better understand those results, and to reveal the implication for the above physiological function of sugar, it is necessary to obtain information concerning the microscopic nature of the sugar–water interaction.

A computer simulation is appropriate for this purpose. Recently, a molecular-dynamics (MD) study of an aqueous solution of trehalose has been reported by Donnamaria et al.[19] According to that report, the addition of trehalose only slightly modifies the hydrogen-bond network and the water dynamics. This is, at first glance, inconsistent with the experimental results mentioned above. The radial distribution function of water molecules around each hydroxy group of the sugar (given in Fig. 5 of Ref. 19) exhibited an appreciably broad first peak. This is again inconsistent with previous molecular-dynamics studies of aqueous solutions of glucose and maltose.[20,21] These problematic points should be clarified in order to deduce conclusive information concerning the hydration ability of trehalose.

Here, we describe the results for a total of three MD simulations, including trehalose and two conformers of maltose in aqueous solution. The simulation data show that trehalose has a higher hydration ability than does maltose, which is consistent with the available experimental data. Finally, we discuss the implication for the biological function of treha-

lose.

Computational Details

Molecular-dynamics simulations were carried out using the Amber 4.0 program[22] installed on a TITAN 3000V computer. The potential energy function used for the sugar molecules was a typical Amber-type molecular-mechanics energy function without any special tuning for sugar. However, the original Amber data base does not possess the force filed parameters necessary to bend oxygen–carbon–oxygen (OS–CT–OS and OH–CT–OS according to the notation of the Amber program). Here, the force constant and equilibrium bond angle for this angle were determined so as to correctly reproduce the X-ray structure of glucose. Then, the initial parameter set, including the force constant and equilibrium bond angle, was taken from those for analogous atom sequences, such as O–CT–OH and O–CT–O. Both values of the force constant and equilibrium bond angle were changed at a 0.5 interval over a range of ±5.0 from the corresponding initial value. With each set of the given parameter values, the geometry of glucose was optimized and the result was compared with the X-ray structure. Consequently, for both OS–CT–OS and OH–CT–OS, the optimized values for the force constant and equilibrium bond angle were 80.0 kcal rad^{-2} and 108.5°, respectively. The atomic charges (Table 1) were determined so as to reproduce the molecular electrostatic potential derived from the MNDO wave function of each solute, using the MOPAC 6.0 program.[23] Hereafter, these charges are called MNDO-ESP charges.

To confirm the reliability of the force-field parameters used, we obtained an adiabatic potential map concerning the rotation of the glycosidic bonds of trehalose (data not shown). The rotation was expressed as a function of two dihedral angles (ϕ and ψ) defined as H^1–C^1–O^1–$C^{1'}$ and C^1–O^1–$C^{1'}$–$H^{1'}$, respectively (Fig. 1a). The global minimum appeared at $\phi = -60°$ and $\psi = -60°$. According to an X-ray study of anhydrous trehalose.[24] ϕ and ψ are −58.2° and −59.0°, respectively. Thus, the present calculation satisfactorily reproduces the the experimental structure.

A recent molecular-mechanics study has indicate that maltose has several low-energy conformations in vacuum.[25] In the present study, two sets of initial values were given for glycosidic dihedral angles of ϕ and ψ, defined as H^1–C^1–O^1–$C^{4'}$ and C^1–O^1–$C^{4'}$–$H^{4'}$, respectively (Fig. 1b). One is (ϕ, ψ) = (4.9, 13.3), corresponding to the crystal structure.[26] The other is (ϕ, ψ) = (4.9, 148.3). Hereinafter, these conformers are called maltose A and B, respectively. The angle ψ of maltose B is greatly shifted from that of maltose A. According to optical-rotation and NMR NOE studies,[27,28] maltose A is more appropriate as a model of maltose in the solution state than maltose B. An early study using a continuum solvation model has suggested that a con-

Table 1. Partial Atomic Charges for Trehalose and Maltose

Atom	Trehalose	Maltose	
		Nonreducing	Reducing
C^1	0.26	−0.15	0.44
H^1	0.15	0.15	0.15
O^1	−0.38	−0.53	-0.69
$H(O^1)$ [a]	—	—	0.44
C^2	0.25	0.14	0.14
H^2	0.05	0.15	0.15
O^2	−0.69	−0.70	−0.70
$H(O^2)$ [a]	0.46	0.46	0.46
C^3	0.11	0.14	0.14
H^3	0.11	0.07	0.07
O^3	−0.69	−0.71	−0.71
$H(O^3)$ [a]	0.44	0.43	0.43
C^4	0.21	0.26	0.26
H^4	0.08	0.21	0.12
O^4	−0.68	−0.68	—
$H(O^4)$ [a]	0.42	0.45	—
C^5	0.02	0.08	0.08
H^5	0.10	0.11	0.11
O^5	−0.44	−0.44	−0.44
C^6	0.13	0.24	0.24
H^6A [b]	0.05	0.05	0.05
H^6B [b]	0.05	0.05	0.05
O^6	−0.59	−0.69	−0.69
$H(O^6)$ [a]	0.39	0.44	0.44

a) $H(O^n)$ indicates the hydrogen atom of the nth hydroxy group.
b) Hydrogen atoms of the methylene group.

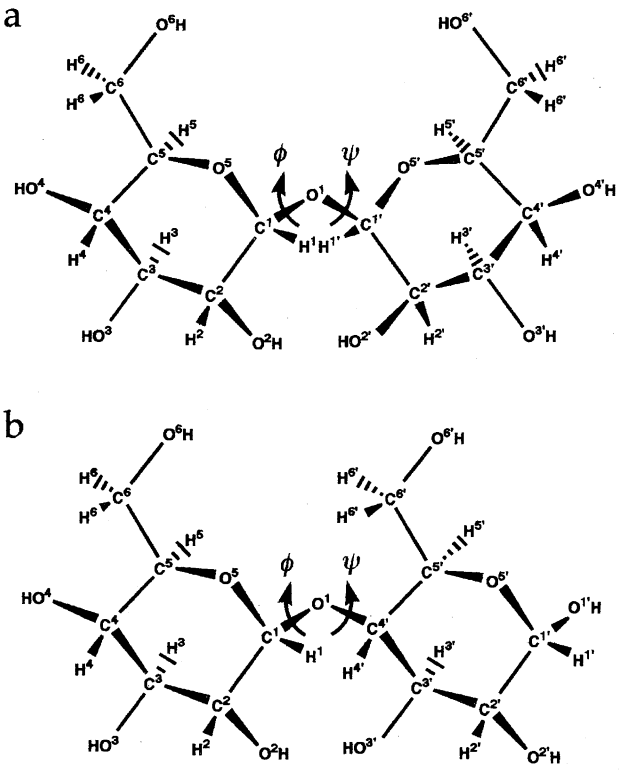

Fig. 1. The numbering of atoms and the definition of the glycosidic dihedral angles ϕ and ψ. a: Trehalose. The angles ϕ and ψ were defined as H^1–C^1–O^1–$C^{1'}$ and C^1–O^1–$C^{1'}$–$H^{1'}$, respectively. b: Maltose. The angles ϕ and ψ were defined as H^1–C^1–O^1–$C^{4'}$ and C^1–O^1–$C^{4'}$–$H^{4'}$, respectively.

formation near (ϕ, ψ)=(−40, −160), nearly equal to those of maltose B, is electrostatically stabilized in solution.[29] However, this is unacceptable according to a recent optical rotation study.[27] Thus, maltose B should be regarded as being a hypothetical conformer. As described later, a comparative study of these conformers provides information on the effects of the backbone conformation on the hydration property of this sugar.

In both trehalose and maltose, the other geometrical parameters were taken from the respective crystallographic data.[26,30] The initial geometries of maltoses A and B are identical to each other, except for the angle of ψ. Before a respective MD run, all of the geometrical parameters were optimized using the "energy minimization" option of the Amber program.

The initial coordinates for the sugar–water systems were prepared as follows. First, the sugar molecule was put into a cubic box containing TIP3P water molecules equilibrated at 298 K. Those water molecules with oxygen atoms, whose van der Waals radii overlapped any of the atoms in the sugar, were then discarded from the system. The box length was given a value of 24.64 Å. The concentration and density of the resulting solution are summarized in Table 2. Before starting a molecular-dynamics simulation, the energy minimization using the conjugated gradient method was performed so as to relax any steric hindrances artificially produced by the initialization procedure.

All of the simulations were carried out under the NVT ensemble. Periodic boundary conditions were employed, and the cutoff radius for long-range interactions was 12.32 Å. All of the C–H bond lengths were kept fixed at their crystallographic values using the SHAKE procedure. The equation of motion was integrated with a step size of 1 fs. The system was equilibrated for 10 ps, and the subsequent 40 ps trajectory was used for data collection. The trajectory data were saved at a 10 fs interval.

Data Analysis In this study, a two-dimensional distribution function was introduced to reveal the spatial distribution of water oxygen atoms around each hydroxy oxygen atom of sugar. The oxygen–oxygen pair distribution (g_{O-O}) was given as a function of two variables, that is, the O–O distance (r) and the angle (θ) made between the OH vector of a given sugar hydroxy group and the vector connecting the hydroxy oxygen atom and a water oxygen atom. The definition of these variables is shown in Fig. 2. As can be seen from this figure, the value of θ is around zero when the sugar hydroxy group acts as a proton donor in forming a hydrogen bond with the water molecule. When this hydroxy group is a proton acceptor, the angle of θ is about 110°, a value which equals the angle made between the OH vector and a lone pair of the hydroxy oxygen. If both types of hydrogen bond occur at r=2.8 Å, a two-dimensional contour map of g_{O-O} (r, θ) should have two peaks on the line r=2.8 Å. However, the presence of a peak at around (r, θ)=(2.8, 110) may not necessarily assure the occurrence of ideal hydrogen bonding, which means that an OH vector of water is parallel to the vector connecting the water oxygen and the sugar hydroxy oxygen. This point does not cause any substantial problem in the subsequent discussion.

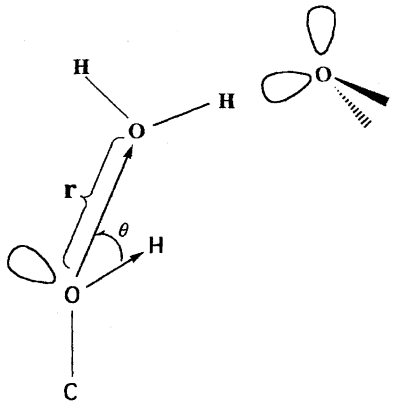

Fig. 2. Definition of variables appearing in a two dimensional pair distribution function. A hydroxy group of sugar is directly hydrogen bonded to a nearest-neighbor water, which is further hydrogen bonded to a next nearest-neighbor water. The variable r is defined as the length of the vector directing from the oxygen atom of this hydroxy group to that of the nearest-neighbor water. The variable θ is defined as the angle made between this vector and the O–H vector of the sugar.

The self-diffusion coefficients were obtained by monitoring the displacement of a molecule as a function of time and using the Einstein relation

$$D = \lim (\mathrm{d}/\mathrm{d}t) \times \langle |r_i(t) - r_i(0)|^2 \rangle.$$

The value for bulk water was obtained from an MD simulation for a system containing 216 TIP3P water molecules in a unit cell. For a solution simulation of sugar, the diffusion coefficient for water molecules was estimated for each hydration shell around the hydroxy oxygen atom of sugar. First, from the trajectory data at a given sampling time, we searched water molecules whose oxygen atom is located within 3.5 Å from a given hydroxy group of sugar. Then, the displacements of those water molecules up to the next sampling time were calculated and their mean-square value was obtained.

Table 2. Simulation Conditions for the Aqueous Solution of Trehalose, Maltoses A and B

Property	Trehalose	Maltose A	Maltose B
Molecular weight	342	342	342
No. of water	419	418	414
Concentration /M	0.11	0.11	0.11
/mol kg^{-1}	0.13	0.13	0.13
Density /g cm^{-3}	0.875	0.873	0.865

Such a procedure was repeated for each sampling interval (0.1 ps), and the final mean-square displacement was given as an average value over all of the sampling intervals.

Results

Structural Fluctuation Figures 3a and 3b show the trajectories of the glycosidic dihedral angles of trehalose. The angle ϕ fluctuates around one conformation, but only for a brief (13—15 ps) period. Its mean value is $-37.6°$ with an rms fluctuation of 13.2°. The angle ψ fluctuates around one mean value throughout the data-collection period; the mean value and the rms fluctuation are $-38.3°$ and 12.7°, respectively. On the other hand, the fluctuations of the glycosidic dihedral angles of maltose A (Figs. 3c and 3d) are apparently larger than those for trehalose. In particular, the angle ϕ shifts to 30° from $-45°$ at 28 ps and returns to the original value at 35 ps. During this period, the fluctuation of the angle ψ also becomes larger. These results may imply that in maltose A the potential wells located near (ϕ, ψ)=(0, 0) are relatively shallow. In fact, it has been reported that an adiabatic potential-energy surface for maltose exhibits a complicated structure in the region of (ϕ, ψ)=(-60—40, -40—20); there are at least three wells.[21]

Figure 4 shows the trajectories of the dihedral angle (ω), defined as C^4–C^5–C^6–O^6. The exocyclic hydroxymethyl groups of a glucopyranose ring can exist in three nominal orientations relative to O^5 and C^4, respectively. These orientations are usually designated GG, GT, and TG, corresponding to an angle ω of 60°, 180°, and $-60°$, respectively. According to this notation, one exocyclic hydroxymethyl group of trehalose (Fig. 4a) undergoes a series of conformational transition of TG→GG→TG during the data-collection period, while the other (Fig. 4b) exhibits a more complicated pattern with a transition of TG→GT→TG. On the other hand, both hydroxymethyl groups of maltose A experience less frequently such a conformational transition than do those of trehalose, as shown in Figs. 4c and 4d. In particular, the exocyclic hydroxymethyl group of the reducing residue stays in the GG conformation over the entire trajectory, which is in good agreement with a previous report on a solution simulation of maltose.[21] As described later, the orientation of this primary hydroxy group is thought to be stabilized by a local electrostatic force capable of overcoming the solvation force.

Hydration From the obtained trajectory data, we calculated the radial-distribution function for water oxygen atoms

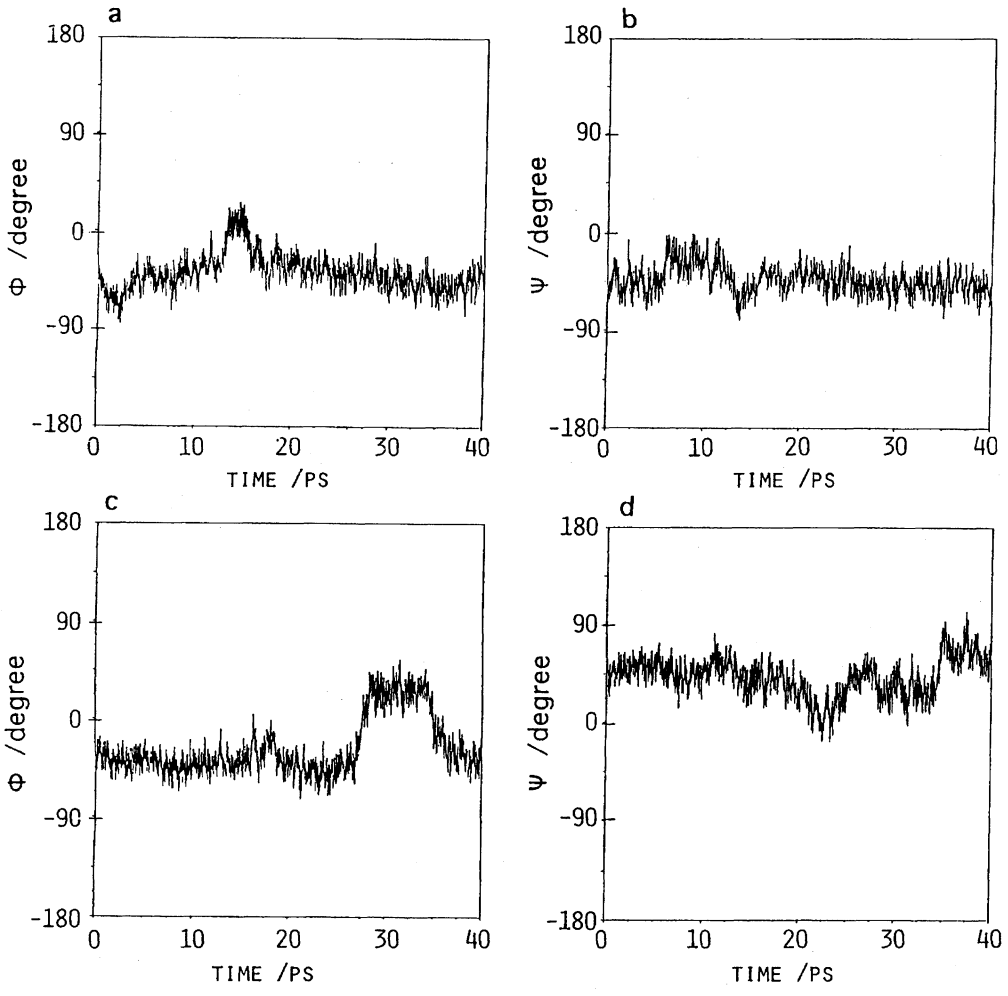

Fig. 3. History of the dihedral angles ϕ and ψ. a and b: Trehalose. c and d: Maltose A.

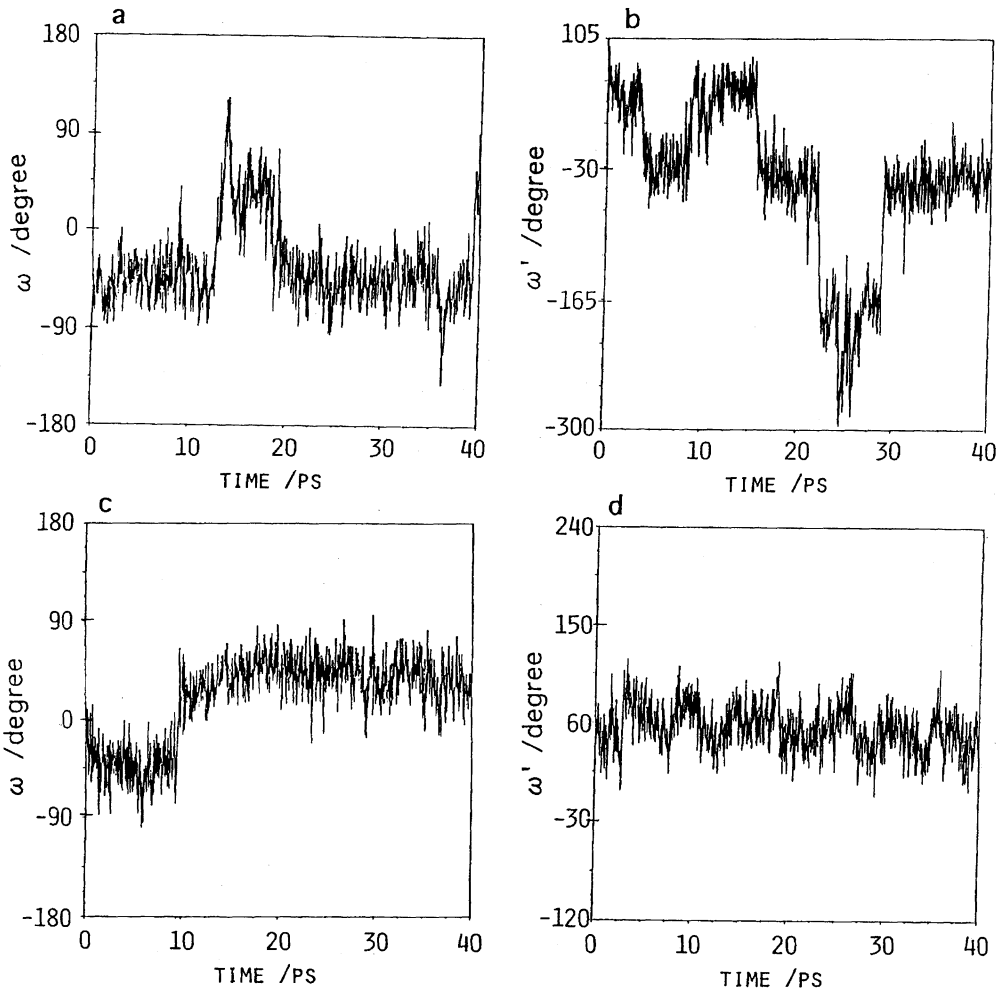

Fig. 4. History of the dihedral angle ω describing the orientation of the exocyclic hydroxymethyl group. a and b: Trehalose. c and d: Maltose A. The angles ω and ω' represent the orientations of the hydroxymethyl groups in the nonreducing and reducing rings, respectively.

around each of the polar groups. The distribution functions around the hydroxy oxygen atoms exhibited sharp, narrow first peaks at around 2.8 Å and deep first minima at around 3.5 Å, as exemplified in Fig. 5a. In addition, the second peak appeared near to 5 Å. As is well-known, the TIP3P potential used here produces less-structured water: In the radial-dis-

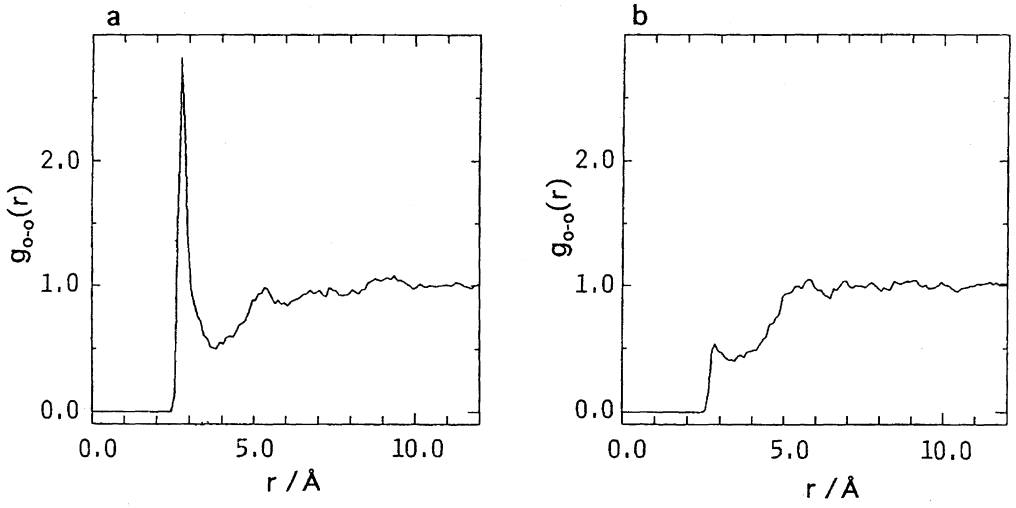

Fig. 5. Oxygen–oxygen radial distribution functions obtained from the MD trajectory of an aqueous solution of trehalose. a: The O^3 hydroxy oxygen atom. b: The O^5 ring oxygen atom.

tribution function there are no apparent first minimum and second peak.[31] Combining this fact with the present calculated data for sugar solutions, it can be said that in trehalose the hydration shell around each hydroxy group is considerably structured compared with that of pure water.

As can be seen from Fig. 5b, the ring oxygen O^5 of trehalose is very weakly hydrated: The first peak is almost collapsed. A similar feature was also found in the results for the other ring oxygen and the glycosidic linkage oxygen atoms of trehalose and maltose A, consistent with other simulation studies.[19—21]

The most striking difference in hydration between trehalose and maltose A was found at the $O^{6'}$ position (Fig. 6). The first peak of the radial distribution function around the $O^{6'}$ oxygen of maltose A (Fig. 6b) is apparently smaller than that for the O^6 oxygen (Fig. 6a) and the corresponding data for the O^6 and $O^{6'}$ sites of trehalose. Table 3 lists the integral of the first peak of the radial-distribution function around each oxygen atom, giving the number of nearest-neighbor water oxygen atoms. As can be seen, the $O^{6'}$ oxygen (the O^6 oxygen of the reducing ring) of maltose A is less hydrated than the other hydroxy oxygen atoms of maltose A and trehalose. This is related to the anomalous behavior for the orientational dynamics of the $O^{6'}$ hydroxymethyl group mentioned above.

Table 3. The Intensity of the First Peak in the Radial Distribution Function

Atom	Trehalose [a]	Maltose A	
		Nonreducing	Reducing
O^1	—	—	4.54
O^2	4.26	3.99	4.17
O^3	4.77	4.77	4.40
O^4	3.59	4.39	—
O^6	4.24	3.93	3.18
Average	4.22	4.17	
Observed n_f [b]	3.98	3.25	
n_h [c]	15.3	14.5	

a) Average values for the two glucose rings. b) Number of unfrozen water per residue cited from Ref. 16. c) Number of hydration water cited from Ref. 17.

The hydration structure around each hydroxy group can be examined in more detail using a two-dimensional pair-distribution function, as previously defined. Figure 7 shows the data for four hydroxy groups belonging to one of the two glucose rings of trehalose. In all of the cases, two peaks are present along with a line of r=2.8 Å. One is located at around θ=15°, and the other around 110°. As expected, such a double-peak pattern also appears in pure TIP3P water (Fig. 8). Thus, all of the hydroxy groups of trehalose act as both a hydrogen-acceptor and -donor in a similar way to the hydroxy group of water.

For maltose, similar results were obtained for all of the hydroxy oxygen sites of the nonreducing ring and for the $O^{1'}$, $O^{2'}$, and $O^{3'}$ oxygen sites of the reducing ring. However, the $O^{6'}$ oxygen site again exhibited an anomalous behavior (Fig. 9): No peak was observed at around θ=110°. It is thus evident that the $O^{6'}$ hydroxy group acts as only a hydrogen donor, which is responsible for the weaker intensity of the first peak in the radial distribution function mentioned above.

The two-dimensional pair distribution function also provides information about the water structure around the second hydration shell. On the basis of a geometrical consideration of the I_h structure of ice, the oxygen atom of the next nearest-neighbor water exists at r=4.7 Å and the angle θ should be shifted by 35° from the value for the nearest-neighbor water. As can be seen from Fig. 7, there are some peaks in the region of r=3.5—5 Å, except for the O^2 hydroxy oxygen. However, the locations of these peaks do not necessarily satisfy the above geometrical conditions for the ice-like structure. For example, although the second-shell peak for the O^4 site may satisfy the condition for θ, the value of r (=3.7—3.8 Å) is fairly small compared with the ideal one (4.7 Å). The lack of a second peak at the O^2 (and $O^{2'}$) site suggests that the formation of the ice-like structure is greatly disturbed. From these finding, it may be said that the water structure near to

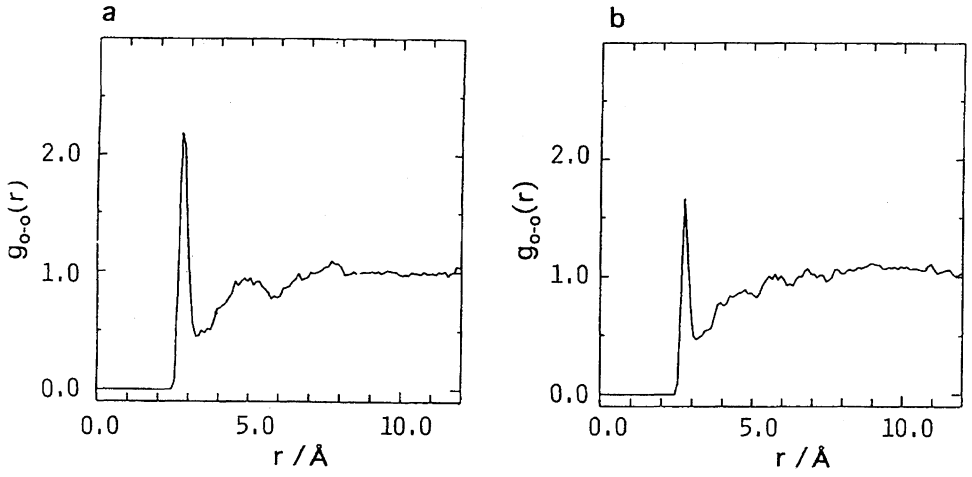

Fig. 6. The oxygen–oxygen radial distribution functions for the O^6 and $O^{6'}$ hydroxy oxygen atoms of maltose A.
a: The O^6 oxygen atom. b: The $O^{6'}$ oxygen atoms.

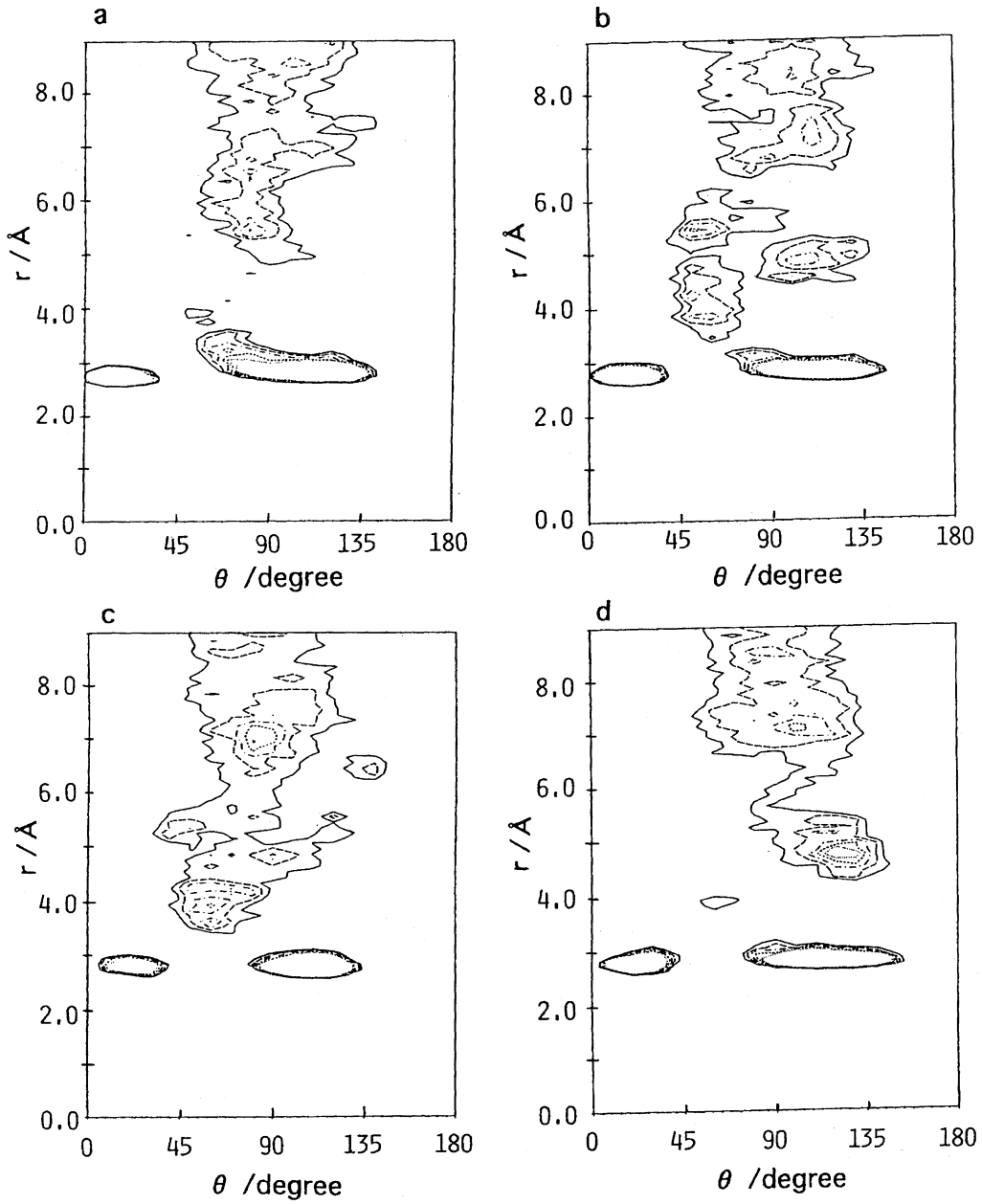

Fig. 7. Representative two dimensional pair distribution functions for trehalose. a: The O^2 oxygen atom. b: The O^3 oxygen atom. c: The O^4 oxygen atom. d: The O^6 oxygen atom.

trehalose is different from the I_h structure of ice.

Similar results were obtained for maltose A, except for a few points. In maltose A, the second shell peaks were not found at the O^2 and $O^{3'}$ sites (Fig. 10). Combining this result with those for the O^2 (and $O^{2'}$) site of trehalose, it has been shown that a hydrogen-bonding network is difficult to develop near to the glycosidic linkage. One of the most characteristic feature in maltose A was again found for the $O^{6'}$ site. The water distribution in the region of r=3.5—5 Å is similar to that of pure water (Fig. 8). This finding indicates that the water structure around this site is less perturbed due to the defect of the hydrogen-bonding network mentioned above.

Effects of the Backbone Structure. The simulation for maltose B provides an invaluable insight into the origin of the anomalous hydration of the $O^{6'}$ hydroxy group observed for maltose A. The two-dimensional pair-distribution functions for the O^6 and $O^{6'}$ hydroxy oxygen atoms of maltose B are shown in Figs. 9c and 9d, where one can see a double-peak pattern on the line r=2.8 Å. In addition, the $O^{6'}$ hydroxymethyl group frequently undergoes conformational transitions among the GG, GT, TG rotamers during the entire period of data collection (data not shown). The mean ϕ and ψ angles of maltose B were −32.9° (rms fluctuation=9.4°) and −174.0° (rms fluctuation=9.8°), respectively. These values are very different from those of maltose A. In maltose B, the O^6 hydroxymethyl group is placed at the position where the $O^{6'}$ group is inverted with respect to the glycosidic oxygen atom. Due to this symmetrical arrangement, both groups are equivalently hydrated. In maltose A, the

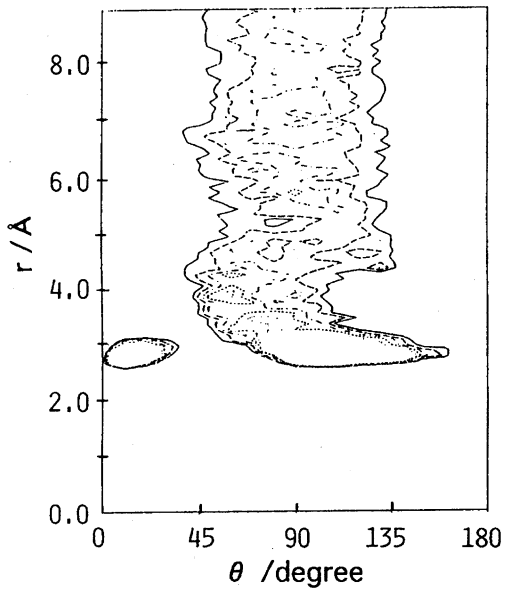

Fig. 8. The two dimensional pair distribution function for pure TIP3P water.

$O^{6'}$ group is surrounded by a relatively-hydrophobic cleft formed by the glycosidic linkage and the ring oxygen of the nonreducing residue, is thus less hydrated.

Snap shots at 20 ps (Fig. 11), taken from the MD trajectories, show selected water molecules located within 5 Å from the glycosidic oxygen atom. In maltose A, water molecules are apparently excluded from the region including the glycosidic bond, in contrast to the cases of trehalose and maltose B.

Self-Diffusion Coefficient of Water. Each of the present MD simulations contained more than four hundred water molecules (Table 2), and their major fraction was not dynamically constrained on the solute. Thus, a diffusion coefficient averaged over all of the water molecules exhibited no obvious tendency of a restricted-translational motion that would be caused by an interaction with sugar. Then, the diffusion coefficient was calculated for the water molecules located in each of the first solvation shells around the hydroxy oxygen atoms of sugar. Table 4 lists the value of the diffusion coefficient for each solvation shell and that for pure TIP3P water at 298 K. The calculated value for pure water was 3.12 $m^2 s^{-1}$, somewhat larger than the experimental value (2.3×10^9 $m^2 s^{-1}$) at 298 K.[32] In the three sugar–water systems, the magnitude of the diffusion coefficient varies depending on the location of the water molecules. Such site-dependent variations of the diffusion coefficients may be partially attributed to statistical fluctuations due to inadequate sampling.[20] In fact, it can not take a long sampling time to give sufficiently-quantified data for these diffusion coefficients, because water molecules are exchanged between the first hydration shell and the outer region. Thus, we do not refer to details of the site dependency. Instead, the values averaged over the OH sites are compared between trehalose and maltose. For both sugars, the translational motion of the water molecules located in the first solvation shell is significantly restricted compared with that of pure water. In addition, the lowering of motion is somewhat larger in the trehalose solution than in the maltose solution.

Discussion

The present simulation results indicate that both of trehalose and maltose cause an appreciable amount of structural and dynamical modification to their surrounding aqueous medium. In what follows, we compare these results with available experimental data.

Table 3 lists the number (n_f) of unfrozen water molecules per residue and the hydration number (n_h) obtained from ultrasound measurements. Unfrozen water is strongly bound to the solute, and thereby could not participate in the formation of the I_h structure of ice. The hydration number (n_h) is given based on an observation of the partial molar compressibility ($K_s°$) of an aqueous solution of sugar.[17] The increase in n_h corresponds to the increase in the absolute value of $K_s°$, which is also correlated with the degree of structural unfitting of the solute to bulk water.[17] Although these experimental data have different physical meanings from each other, both indicate that trehalose more strongly modifies the surrounding water structure than does maltose. According to the present simulation results, the average number of hydration water molecules per residue is somewhat larger in trehalose than in maltose A, which is attributed mainly to the less hydration at the $O^{6'}$ site of maltose. In addition, the results of the two-dimentional distribution functions suggested that the

Table 4. Self-Diffusion Coefficients D ($10^9 \times m^2 s^{-1}$) of Water around Each OH Group

Site	Trehalose [a]	Maltose A		Maltose B	
		Nonreducing	Reducing	Nonreducing	Reducing
O^1	—	—	1.90	—	2.01
O^2	2.02	2.04	2.13	2.13	2.09
O^3	1.84	1.76	1.78	2.17	2.00
O^4	1.68	2.02	—	2.03	—
O^6	1.86	1.78	1.87	1.92	1.77
Average [b]	1.85	1.90	1.92	2.06	1.96
Pure water		3.10			

a) Average values for the two glucose rings. b) Average values for the four kinds of OH sites.

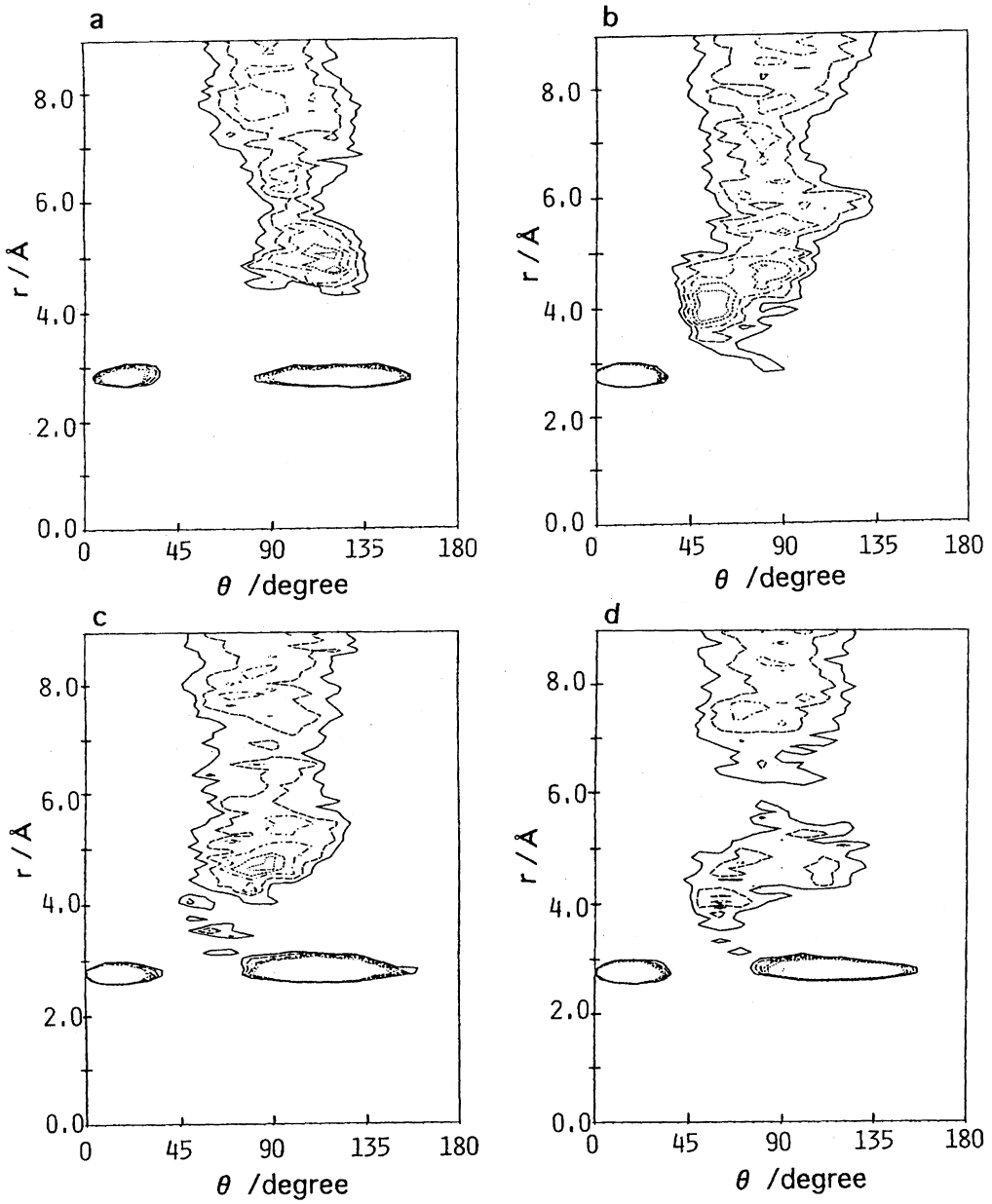

Fig. 9. Two dimensional pair distribution function for maltoses A and B. a : The O^6 oxygen atom of maltose A. b : The $O^{6'}$ oxygen atom of maltose A. c : The O^6 oxygen atom of maltose B. d : The $O^{6'}$ oxygen atom of maltose B.

water structure around the hydroxy groups of these sugars is different from the ice-like structure, which is equivalent to the so-called tridymite structure of bulk water. Consequently, the simulation successfully reproduces the tendency of the experimental data, namely the higher potentiality of trehalose as a water-structure marker.

We now consider the origin of anomalous hydration at the $O^{6'}$ site of maltose A. When the $O^{6'}$ hydroxymethyl group of maltose A takes the GG orientation, its oxygen atom is 2.5—3.0 Å distant from the $O^{4'}$ and $H^{4'}$ atoms. As can be seen from Table 1, the asymmetric carbon and its neighboring hydrogen possess modest amounts of positive charge. As a result, the GG orientation could be stabilized by a coulombic attraction between the hydroxy oxygen and these atoms. Therefore, the lone pair of $O^{6'}$ is stabilized by such an intramolecular interaction, rather than by hydrogen bonding with a surrounding water molecule. This clearly explains the anomalous behavior of the trajectory data (Fig. 4d) and the two-dimensional distribution function (Fig. 9b) for the $O^{6'}$ hydroxy group.

Our recent ^{17}O NMR study has indicated that the aqueous solution of trehalose exhibits a larger dynamic hydration number (n_{DHN}) than does that of maltose.[16] We define n_{DHN} as follows:[33]

$$n_{DHN} = n_h(\tau_c^h/\tau_c^\circ - 1),$$

where n_h is the hydration number, τ_c^h and τ_c° are the rotational correlation times of the water molecules in the hydration shell and of bulk water, respectively. The larger is n_{DHN}, the more is the motion of water in the hydration

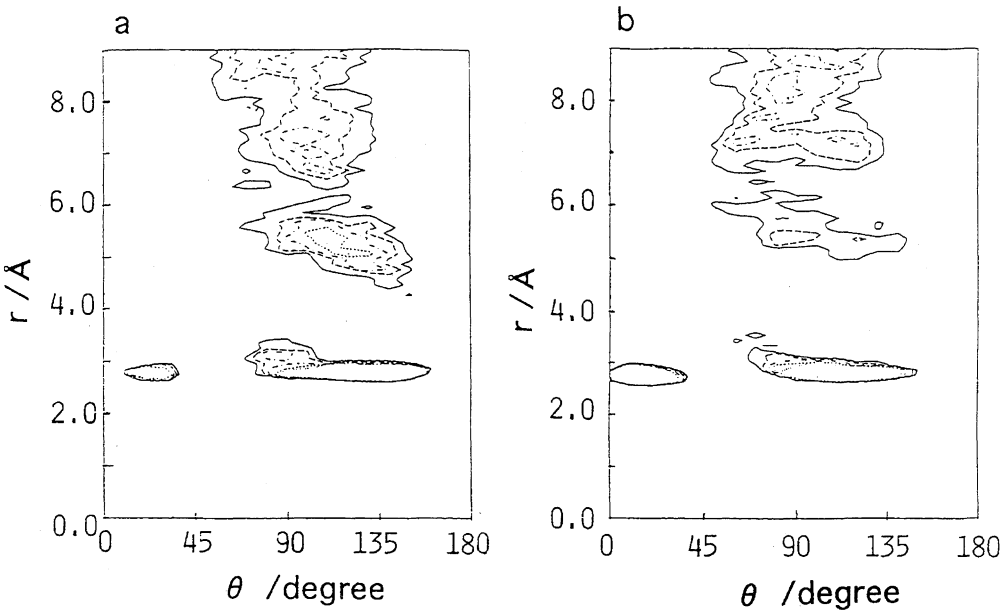

Fig. 10. Two dimensional pair distribution function for maltoses A. a: The O^2 oxygen atom. b: The $O^{3'}$ oxygen atom.

shell restrained. According to our measurements,[16] n_{DHN} for a trehalose solution was 48.3, and that for a maltose solution was 27.2. The present simulation data alone cannot be directly used to evaluate n_{DHN}, because the rotational correlation time was not calculated. However, it is known that $\tau_c^h/\tau_c^\circ \fallingdotseq \tau_D^h/\tau_D^\circ$ is fulfilled for an aqueous solution of sugar, where τ_D is the correlation time for translational diffusion.[33] Based on this assumption, we can estimate the relative order of n_{DHN} for trehalose and maltose solutions. The self-diffusion constant (D) is inversely proportional to τ_D. Thus, from the data for the average self-diffusion constants of water molecules in the hydration shell (Table 4), the τ_D^h value for trehalose is expected to be larger than that for maltose A. In addition, the hydration number is larger in trehalose than in maltose A (Table 3). Combining these data, n_{DHN} of trehalose is expected to be larger than that of maltose. This is also consistent with the experimental results.

Therefore, it can be concluded that the present simulation well reproduces the experimental results in both structural (hydration number) and dynamical aspects of hydration.

Donnamaria et al. stated, on the basis of their simulation results, that since the spatial arrangement of the hydroxy groups in trehalose can fit into the so-called tridymite structure (I_h structure of ice) of water, this sugar only slightly disturbs the hydrogen-bonding network of water.[19] However, if this is ture, it seems to be difficult to interpret the experimental data cited above.

The difference between Donnamaria's results and our results is thought to mainly originate from the difference in the partial atomic charges used in the simulation. In this study, the partial atomic charges for trehalose were derived from the MNDO-ESP calculation (Table 1) and TIP3P water was used. On the other hand, the partial atomic charges of trehalose used by Donnamaria's group were derived from an AM1 calculation, which included solvent effects, and SPC/E water was used. The present MNDO-ESP charges for maltose are in good agreement with those employed in Ref. 21, which reported on solution simulations of maltose, and gave a radial-distribution function similar to the present results. In a comparison with the MNDO-ESP charge, the AM1 charges considerably underestimate the polarization of C–O and O–H bonds. It should be noted that the atomic charge of the hydroxy oxygen was −0.25——−0.35 (Table 1 in Ref. 19). If such a small amount of charge is used for sugar, the hydrogen bonding between the hydroxy group of the sugar and water is expected to be considerably weaker than water–water hydrogen bonding; this is because in the SPC/E water the oxygen possesses a charge of about −0.8,[34] which is nearly equal to the value of the TIP3P water. This may account for the fact that the oxygen–oxygen radial distribution functions given by Donnamaria et al. exhibit considerably broad first peaks, probably leading to their conclusion which insists that trehalose gives no apparent modification to the surrounding water structure.

We recently measured the amount of bound water in freeze-dried yeast cells using ^{1}H NMR spectroscopy.[35] A surprising finding in that report was that by accumulating intracellular trehalose the amount of bound water drastically increased compared with that in yeast cells lacking this sugar. It has been proposed that the increase in bound water essentially contributes to maintaining the structural and functional integrity of proteins and membranes in cells. Trehalose should be of greater advantage in such a protecting mechanism, because this sugar has a higher ability to increase bound water molecules. Such a property originates from the fact that all of its hydroxy groups can participate in hydrogen bonding with water through both roles of a proton donor and an acceptor.

Conclusion

In the present MD simulation, we found an appreciable difference in the hydration ability between trehalose and

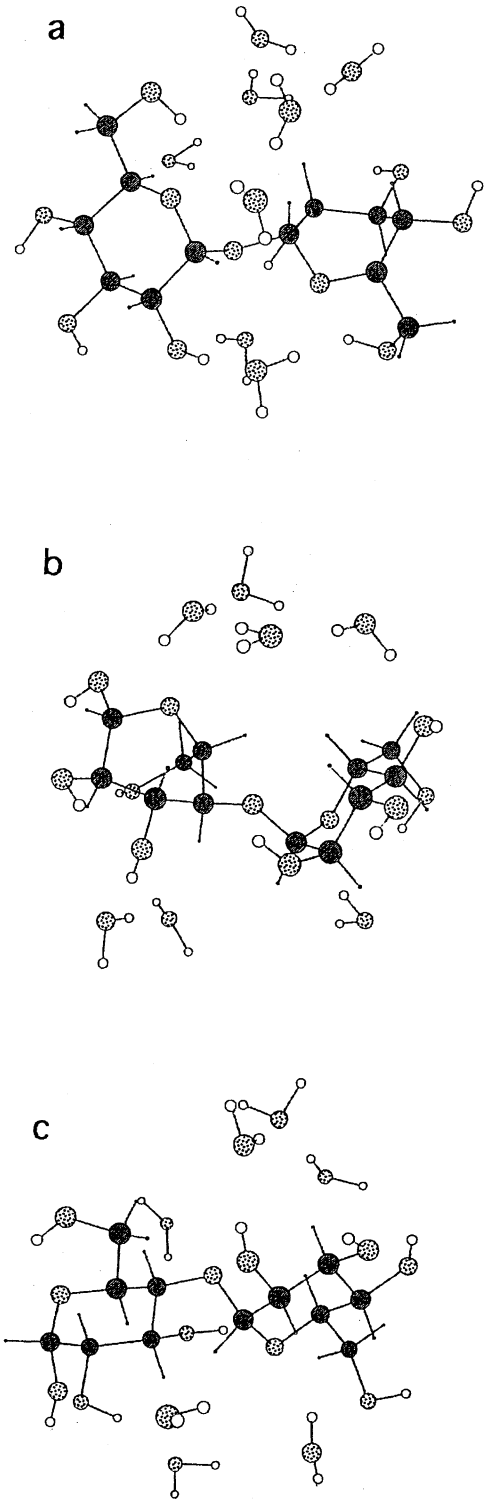

Fig. 11. Snap shots at 20 ps from the MD trajectories. a : Trehalose. b : Maltose A. c : Maltose B.

maltose. In trehalose, all of the hydroxy groups can act as both a proton donor and an acceptor in forming hydrogen bonds with the surrounding water molecules. In maltose, a defective hydrogen bond was found at the $O^{6'}$ position. As a result, trehalose causes slightly larger perturbations to the surrounding water structure than does maltose, consistent with the available experimental data. The superior hydration ability of trehalose would be advantageous for the protecting mechanism mentioned above. To further understand the function of this sugar as a stress protectant, it is of great interest to apply MD simulations to systems involving proteins or membranes in the future.

The molecular-orbital calculation was carried out using computer systems of the Institute for Molecular Science (IMS), Okazaki, Japan. We thank the computer center of IMS.

References

1) T. Hottiger, T. Boller, and A. Wiemken, *FEBS Lett.*, **220**, 113 (1987).
2) T. Hottiger, T. Boller, and A. Wiemken, *FEBS Lett.*, **255**, 431 (1989).
3) C. De Virgilio, U. Simmen, T. Hottiger, T. Boller, and A. Wiemken, *FEBS Lett.*, **273**, 107 (1990).
4) C. De Virgilio, P. Piper, T. Boller, and A. Wiemken, *FEBS Lett.*, **288**, 86 (1991).
5) T. Hottiger, C. De Virgilio, W. Bell, and A. Wiemken, *Eur. J. Biochem.*, **210**, 125 (1992).
6) A. Hino, K. Mihara, K. Nakashima, and H. Takano, *Appl. Environ. Microbiol.*, **56**, 1386 (1990).
7) S. Nwaka, M. Kopp, M. Burgert, I. Deuchler, I. Kienle, and H. Holzer, *FEBS Lett.*, **344**, 225 (1994).
8) P. van Dijck, D. Colavizza, P. Smet, and J. M. Thevelein, *Appl. Environ. Microbiol.*, **61**, 109 (1995).
9) B. Roser, *Trend. Food Science Technol.*, **7**, 166 (1991).
10) T. Hirata, H. Yokomise, T. Fukuse, K. Inui, K. Yagi, S. Hitomi, and H. Wada, *Thorac. Cardiovasc. Surg.*, **41**, 51 (1993).
11) J. H. Crowe, L. M. Crowe, J. F. Carpenter, A. S. Rudolph, C. A. Wistrom, B. J. Spargo, and T. J. Anchordoguy, *Biochim. Biophys. Acta*, **947**, 367 (1988).
12) J. H. Crowe, J. F. Carpenter, L. M. Crowe, and T. J. Anchordoguy, *Cryobiology*, **27**, 219 (1990).
13) B. Roser, *Biopharm*, **8**, 47 (1991).
14) F. Franks, R. H. M. Hatley, and S. F. Mathias, *Biopharm.*, **10**, 38 (1991).
15) K. L. Koster, M. S. Webb, G. Bryant, and D. V. Lynch, *Biochim. Biophys. Acta*, **1193**, 143 (1994).
16) H. Kawai, M. Sakurai, Y. Inoue, R. Chujo, and S. Kobayashi, *Cryobiology*, **29**, 599 (1992).
17) S. A. Galema and H. Hoiland, *J. Phys. Chem.*, **95**, 5321 (1991).
18) J. L. Green and C. A. Angell, *J. Phys. Chem.*, **93**, 2880 (1989).
19) M. C. Donnamaria, E. I. Howard, and J. R. Grigera, *J. Chem. Soc., Faraday Trans.*, **90**, 2731 (1994).
20) J. W. Brady, *J. Am. Chem. Soc.*, **111**, 5155 (1989).
21) J. W. Brady and R. K. Schmidt, *J. Phys. Chem.*, **97**, 958 (1993).
22) D. A. Pearlman, D. A. Case, J. C. Caldwell, G. L. Seibel, U. C. Singh, P. Weiner, and P. A. Kollman, "Amber 4.0," University of California, San Francisco (1991).
23) J. J. P. Stewart, "MOPAC ver. 6.0," United States Air Force Academy, 1990.
24) G. A. Jeffrey and R. Nanni, *Carbohydr. Res.*, **137**, 21 (1985).
25) S. N. Ha, L. J. Madsen, and J. W. Brady, *Biopolymers*, **27**, 1927 (1988).

26) M. E. Gress and G. A. Jeffrey, *Acta Crystallogr., Sect. B*, **B33**, 2490 (1977).
27) E. S. Stevens, *Biopolymers*, **32**, 1571 (1992).
28) G. M. Lipkind, V. E. Verovsky, and N. K. Kochetkov, *Carbohydr. Res.*, **133**, 1 (1984).
29) I. Tvaroska, *Biopolymers*, **21**, 1887 (1982).
30) T. Taga, M. Senma, and K. Osaki, *Acta Crystallogr., Sect. B*, **B28**, 358 (1972).
31) W. L. Jorgensen, J. Chandrasekhar, J. D. Madura, R. W. Impey, and M. L. Klein, *J. Chem. Phys.*, **79**, 926 (1983).
32) R. Mills, *J. Chem. Phys.*, **77**, 685 (1973).
33) H. Uedaira, M. Ikura, and H. Uedaira, *Bull. Chem. Soc. Jpn.*, **62**, 1 (1989).
34) H. J. C Berendsen, J. R. Grigeta, and T. P. Straatsma, *J. Phys. Chem.*, **91**, 6269 (1987).
35) M. Sakurai, H. Kawai, Y. Inoue, A. Hino, and S. Kobayashi, *Bull. Chem. Soc. Jpn.*, **68**, 3621 (1995).